J. Fluid Mech. (1997), *vol.* 333, *pp.* 1–21

Instability caused by the coupling between non-resonant shape oscillation modes of a charged conducting drop

By Z. C. FENG

Department of Mechanical Engineering, Massachusetts Institute of Technology, Cambridge, MA 02139, USA

(Received 16 October 1995 and in revised form 9 September 1996)

By examining the modal interaction between two non-resonant shape oscillation modes of a charged liquid drop, we have identified a new route to instability via nonlinear coupling. We present numerical simulation results to show that when shape perturbation of a high-mode number Legendre mode is applied to the drop, the prolate–oblate mode of the drop may grow unbounded. Using multiple-scale analysis, we derive amplitude equations for the high-mode-number shape mode and the prolate–oblate mode to show the nonlinear coupling between the two modes.

1. Introduction

Modal interaction provides a means by which energy transfer takes place between linearly independent modes. In the context of nonlinear dynamics of bubbles and drops, modal interaction greatly affects mass and momentum transfer and often results in hydrodynamic instability and symmetry breaking. For example, Natarajan & Brown (1986) show that the nonlinear coupling between two shape oscillation modes of an inviscid liquid drop leads to energy exchange between the two modes in a periodic fashion. A similar type of nonlinear coupling is shown to occur in the radial mode oscillation and the shape mode oscillation of a gas or a vapour bubble (Ffowcs Williams & Guo 1991; Feng & Leal 1993). For an oscillating bubble, energy transfer from the radial mode to the shape modes causes the spherical shape of the bubble to be unstable. When one of the two resonant modes is forced by an external periodic forcing, it is possible that chaotic bubble oscillation can occur (Mei & Zhou 1991; Feng & Leal 1994).

For linearly independent modes to interact, certain conditions are required. In the drop example given above, the frequencies of the fifth mode and the eighth mode are in one-to-two ratio. For this reason, such modal interactions are called resonant modal interactions.

In the present paper we will show the presence of modal coupling when no apparent frequency relationships exist between the interacting modes. This work is motivated by the paper of Nayfeh & Nayfeh (1992) on nonlinear structural vibrations. Nayfeh & Nayfeh show that nonlinear modal coupling occurs in linearly independent modes whose frequencies are widely spaced. Specifically, they show that energy transfer between two widely spaced modes takes place in the forced vibration of a cantilever beam. This result is very interesting because if the system nonlinearity can be considered weak, energy exchange is expected only if the natural frequencies of the

two modes are approximately in one-to-one, one-to-two or one-to-three ratios. The natural frequencies of the two widely spaced modes considered by Nayfeh & Nayfeh may differ by an order of magnitude. When such modal interactions occur in fluid systems, bubbles and drops in particular, we are interested in its implications for the stability of the fluid flows.

We choose to study the non-resonant modal interaction between the shape oscillation modes of a charged liquid drop as a part of our effort to understand nonlinear dynamics of electrostatically levitated drops (Feng & Leal 1996). Various aspects of the dynamics of a charged conducting liquid drop have been extensively studied. The equilibrium shape and linear stability of a charged drop have been studied by Rayleigh (1882). It is known that a critical charge exists above which the spherical equilibrium shape of the drop is unstable. The critical electric charge is known as the Rayleigh limit. The bifurcation taking place at the Rayleigh limit is studied by Tsamopoulos, Akylas & Brown (1985), Natarajan & Brown (1987), Basaran & Scriven (1989), and Pelekasis, Tsamopoulos & Manolis (1990).

The focus of the present work is on the drop dynamics when the electric charge is near the Rayleigh limit. We attempt to show the presence of non-resonant modal coupling among the shape oscillation modes of the drop. By examining the coupling effect of the shape oscillation of a high mode on the dynamics of the fundamental mode, we uncover a new mechanism for nonlinear instability.

The paper is organized as follows. In the next section, we first present the governing differential equations and the boundary conditions in order to discuss the behaviour of the drop under small perturbations. Then in §3, we describe numerical simulation results of charged-drop shape oscillations. We draw special attention to the coupling between the fundamental shape oscillation mode and another higher mode. In §4, a perturbation method is used to derive amplitude equations for the two interacting modes. The amplitude equations are studied in §5, where the physical meaning of the results is given in terms of the drop dynamics. In §6, we discuss the connection between our results and other related topics.

2. Governing equations and linear solutions

We consider an axisymmetric conducting liquid drop whose volume is equal to that of a spherical drop of radius R. The drop has density ρ, uniform interfacial tension σ, and net electrical charge Q^* in zero gravity. The insulating medium has electric permittivity ϵ_m. We assume that the flow inside the drop is potential flow with the velocity potential ϕ^*. Let V^* denote the electrostatic potential. We choose R, $(\rho R^3/\sigma)^{1/2}$, and σ/R as the characteristic length, time and pressure scales, i.e. we let

$$\phi = \phi^*(\rho/\sigma R)^{1/2}, \quad V = V^*(4\pi\epsilon_m/\sigma R)^{1/2}, \quad Q = Q^*/(4\pi\epsilon_m\sigma R^3)^{1/2}.$$

In standard spherical coordinates, the governing equations for the problem are given by Tsamopoulos *et al.* (1985). The equation governing the hydrodynamic field is

$$\nabla^2\phi = 0 \qquad (0 \leqslant r \leqslant F(\theta,t),\ 0 \leqslant \theta \leqslant \pi), \tag{2.1}$$

where $r = F(\theta,t)$ describes the drop free surface. The equation governing the electric field is

$$\nabla^2 V = 0 \qquad (r \geqslant F(\theta,t),\ 0 \leqslant \theta \leqslant \pi). \tag{2.2}$$

The boundary conditions to be satisfied on the drop surface include the kinematic equation, the normal stress balance equation, the constant electric potential condition,

and the conservation of the total electric charge. The kinematic boundary condition is

$$\frac{\partial \phi}{\partial r} = \frac{\partial F}{\partial t} + \frac{1}{r}\frac{\partial \phi}{\partial \theta}\frac{\partial F}{\partial \theta}. \tag{2.3}$$

The normal stress balance equation is

$$\frac{\partial \phi}{\partial t} + \tfrac{1}{2}(\nabla\phi)^2 + 2H - \tfrac{1}{2}(\boldsymbol{n}\cdot\nabla V)^2 = \Delta P_0 \tag{2.4}$$

where H denotes the mean curvature of the surface and the pressure adjustment ΔP_0 is determined by the constraint of volume conservation of the drop, i.e.

$$\int_0^{\pi} F^3(\theta, t)\sin\theta \mathrm{d}\theta = 2. \tag{2.5}$$

Since we assume the drop to be a conductor, V is a constant on the drop surface, i.e.

$$\boldsymbol{t}\cdot\nabla V = 0. \tag{2.6}$$

The conservation of the total charge on the drop surface gives

$$\int_0^{\pi} (\boldsymbol{n}\cdot\nabla V)F(F^2 + F_\theta^2)^{1/2}\sin\theta \mathrm{d}\theta = -2\mathrm{Q}. \tag{2.7}$$

In addition, we assume that there is no external electric field acting on the drop. Therefore,

$$V = 0 \text{ as } r \to \infty. \tag{2.8}$$

Since we are mainly interested in the coupling phenomenon, we do not include gravity in our formulation. Hence the drop takes a spherical shape at equilibrium. For a charged conducting sphere, the electric potential outside the drop is

$$V_0 = \frac{Q}{r}.$$

When the spherical drop is subjected to shape perturbations, the surface electric charge moves to locations of high curvature. Thus the electric charge is a destablizing force. On the other hand, surface tension smooths out the high curvature. Therefore, the stability of the spherical shape of the drop is dependent on the relative magnitude of these two forces. When the electric charge is below a certain threshold value, the spherical shape is stable. A small initial axisymmetric shape perturbation will excite the shape oscillation of the drop. The shape oscillation can be described as a superposition of Legendre modes. That is

$$F = 1 + \sum_{n=2}^{\infty} \frac{1}{2}\left[z_n \mathrm{e}^{\mathrm{i}\omega_n t} + z_n^* \mathrm{e}^{-\mathrm{i}\omega_n t}\right] P_n(\cos\theta), \tag{2.9}$$

$$\phi = \sum_{n=2}^{\infty} \frac{\mathrm{i}}{2n}\omega_n \left[z_n \mathrm{e}^{\mathrm{i}\omega_n t} - z_n \mathrm{e}^{-\mathrm{i}\omega_n t}\right] r^n P_n(\cos\theta), \tag{2.10}$$

$$V = \frac{Q}{r} + \sum_{n=2}^{\infty} \frac{Q}{2}\left[z_n \mathrm{e}^{\mathrm{i}\omega_n t} + z_n^* \mathrm{e}^{-\mathrm{i}\omega_n t}\right] r^{-(n+1)} P_n(\cos\theta), \tag{2.11}$$

where P_n is the nth-order Legendre polynomial, z_n is the complex amplitude of the nth mode, and ω_n is the shape oscillation frequency of the nth Legendre mode. Rayleigh

(1882) has obtained the formula for the natural frequencies of the shape modes. In the present non-dimensionalization,

$$\omega_n^2 = n(n-1)(n+2)\left[1 - \left(\frac{Q}{Q_R^{(n)}}\right)^2\right] \tag{2.12}$$

where

$$Q_R^{(n)} = 2[(n+2)\pi]^{1/2}. \tag{2.13}$$

Equation (2.12) indicates that apart from the translational mode $n = 1$, the second mode has the lowest natural frequency. Hence we often call this mode the fundamental mode. If the surface electric charge exceeds $Q_R^{(2)}$,the right-hand side of (2.12) becomes negative. It means that the spherical shape is unstable under the second-mode shape perturbation. This critical surface charge is called the Rayleigh limit. In the present non-dimensionalization, $Q_R^{(2)} = 4\pi^{1/2}$. When the electric charge is below the Rayleigh limit, the linear stability theory states that the drop is stable under infinitesimal perturbations. As a problem with moving interfaces, the drop dynamics is nonlinear. The nonlinearity affects the stability of the equilibrium shape in a dramatic way. In particular, instability can set in at subcritical electric charge. Although there exist well-known mechanisms for such nonlinear instability, we present in the following sections a new mechanism of nonlinear instability when the electric charge is subcritical.

3. Numerical simulation results

In this section, we present some interesting observations on the modal interactions and the onset of instability. Our results are based on numerical simulations of the drop dynamics. A detailed description of the numerical simulation method and its implementation are given in Feng & Leal (1996). Briefly stated, the strategy amounts to numerical integration of the following dynamical system:

$$\dot{z} = \phi_t t_z + \phi_n n_z, \tag{3.1}$$

$$\dot{r} = \phi_t t_r + \phi_n n_r, \tag{3.2}$$

$$\dot{\phi} = \tfrac{1}{2}(\nabla\phi)^2 - 2H + \tfrac{1}{2}(\nabla V)^2. \tag{3.3}$$

In the above equations z and r describe the cylindrical coordinates of the nodal points on the free surface of an axisymmetric conducting drop and ϕ is the velocity potential of the drop at the nodal points. These three equations, which are valid on the drop surface, come from the kinematic boundary condition (equations (3.1) and (3.2)) and the dynamic pressure boundary condition (equation (3.3)). If the generator of the axisymmetric drop surface is discretized into n nodes, there are three such equations for each node. Therefore, we have a system of $3n$ first-order ordinary differential equations. For given initial conditions, the Runge–Kutta method is used to advance the time.

The Runge–Kutta method requires the evaluation of the right-hand sides of (3.1)–(3.3) for given values of z, r, and ϕ. Among the terms that need to be evaluated, $\boldsymbol{t} = t_z\boldsymbol{i}_z + t_r\boldsymbol{i}_r$ and $\boldsymbol{n} = n_z\boldsymbol{i}_z + n_r\boldsymbol{i}_r$ are the tangent and the outward normal vectors respectively; $\boldsymbol{i}_z$ and $\boldsymbol{i}_r$ are the two unit vectors in the cylindrical coordinates. All of these quantities are known once the nodal coordinates r and z are known. The evaluation of the right-hand sides of (3.1)–(3.3) also requires the gradients of ϕ and V

on the drop boundary. Both ϕ and V satisfy the Laplace equation; they are defined in the drop interior and exterior respectively. We use the boundary element method (Brebbia, Telles & Wrobel 1984) to solve the normal derivatives of ϕ and V on the drop surface. The tangent derivatives of ϕ are obtained by numerical derivatives of ϕ employing the cubic spline (the tangent derivatives of V are zero for a conducting liquid drop).

In short, we formulate the drop dynamics problem as an initial value problem of a system of ordinary differential equations (3.1)–(3.3). The evaluation of the right-hand sides is done using the boundary element method. This method for solving the potential problem has been found to converge with the mesh refinement. However, as more elements are used, the time steps must be small enough to avoid numerical instability associated with the stiffness of the ordinary differential equations. The mechanism for the numerical instability and the appropriate time steps have been discussed in Feng & Leal (1996) in detail. A time step of 0.0005 is found to be sufficiently small to guarantee numerical stability when up to 80 elements are used.

The non-dimensionalization of Tsamopoulos *et al.* (1985) used here is related to that in Feng & Leal (1996) in the following way:

$$Q_{FL} = (4\pi)^{1/2} Q_{present}.$$

The interesting phenomenon that we are about to describe arises in our numerical study of the dynamics of an electrostatically levitated drop (Feng & Leal, 1996). Specifically, we have been interested in the modal interactions of charged-drop shape oscillations. For a charged drop, several shape oscillation modes can become resonant with each other, i.e. the ratios of their natural frequencies are rational numbers. Typically, the resonant modes exchange energy in a periodic fashion. To show this type of modal interaction, we give our result in terms of the amplitudes of various Legendre modes obtained by taking projections of the drop shape. Figure 1(*a*) plots the amplitudes of the P_2, P_5, and P_8 modes for an uncharged drop. The initial condition corresponds to a drop subjected to a shape perturbation in the fifth mode. The P_5 mode has an initial amplitude of 0.1. Based on equation (2.12), we find that for $Q = 0$, the natural frequency of the eighth mode is exactly twice of that of the fifth mode. It is thus not surprising to see in figure 1(*a*) the slow modulation of the oscillation amplitudes of the P_5 mode and the P_8 mode. The slow amplitude modulation is caused by the resonant energy exchange between the two modes. Since the total energy is conserved, the growth of the oscillation amplitude of one mode is at the expense of the other mode. This type of resonant modal coupling has been analysed by Tsamopoulos & Brown (1984) and Natarajan & Brown (1986).

We note that although the P_2 mode is not resonant with either the P_5 mode or the P_8 mode, the presence of the other modes causes the P_2 mode to experience a small oscillation. When the same simulation is done for a charged drop with charge $Q = 0.915Q_R^{(2)}$ (i.e. $Q_{FL} = 23$), the amplitude of the P_2 mode experiences relatively large oscillations. See figure 1(*b*). In other words, the P_2 mode and the other modes are nonlinearly coupled even though their natural frequencies are not necessarily in resonance.

Next we examine the consequences of such modal coupling on the stability of the drop. We simulate the drop dynamics for a drop with charge $Q = 0.915Q_R^{(2)}$ when the initial shape perturbation of the P_5 mode is 0.135. In figure 2(*a*), we give the amplitudes of the P_2, P_5, and P_8 modes. We observe that the modal coupling leads to the growth of the fundamental mode. During this process, the amplitudes of the other modes (P_1, P_3, P_4, P_6, and P_7) remain relatively small; see figure 2(*b*). Figure

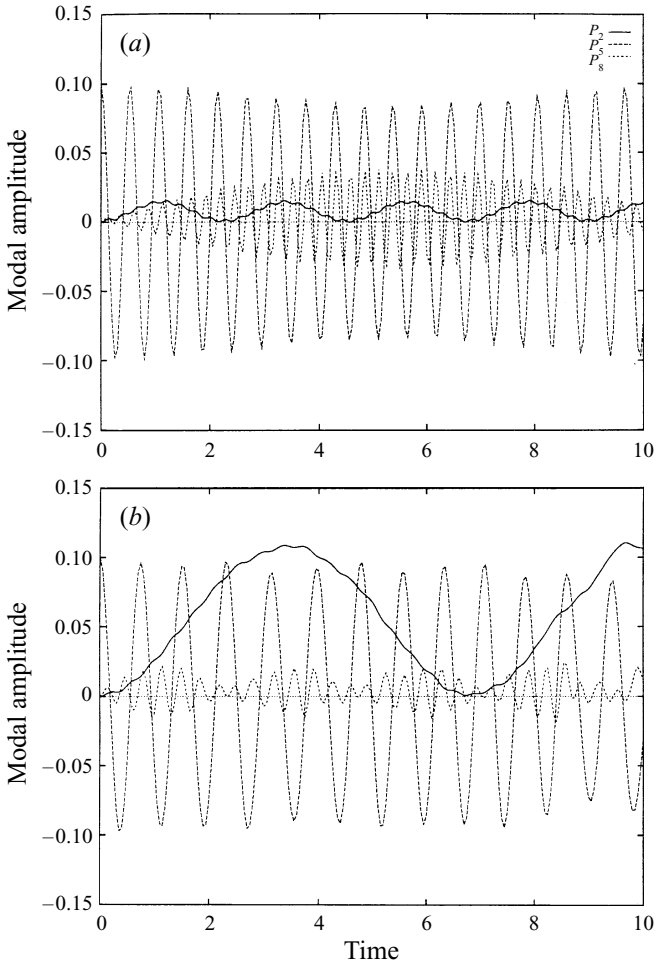

FIGURE 1. The amplitudes of the second, fifth and eighth modes as functions of time for initial shape perturbations in the fifth mode. (*a*) $Q = 0$, (*b*) $Q_{FL} = 23$.

3 shows the drop shapes at equal time intervals. The initial P_5 mode perturbation eventually leads to the elongation of the drop along its symmetry axis (the vertical axis). The last three small figures are the drop shapes on a shorter time interval just before the numerical program stops running. We observe that one of the two poles of the drop develops high velocity. The numerical program stops running because the potential flow solver using the boundary element method encounters a singularity at the high-curvature tip of the drop. Based on our understanding of the dynamics of a charged drop (Feng & Leal 1996), we expect drop breakup to take place subsequently. The plots in figures 2 and 3 are obtained using 40 elements. In order to check the convergences of our numerical program, we repeat the simulations using 50, 60, 70, and 80 elements with almost identical results. For this initial condition, the dimensionless time to the development of a singularity at the drop tip varies between 3.09 and 3.13 depending on the number of elements used. All of our subsequent simulations are done using 40 elements.

As the electric charge approaches the Rayleigh limit, the destablizing effect of the high-mode shape perturbation becomes more pronounced. At $Q = 0.975Q_R^{(2)}$, an

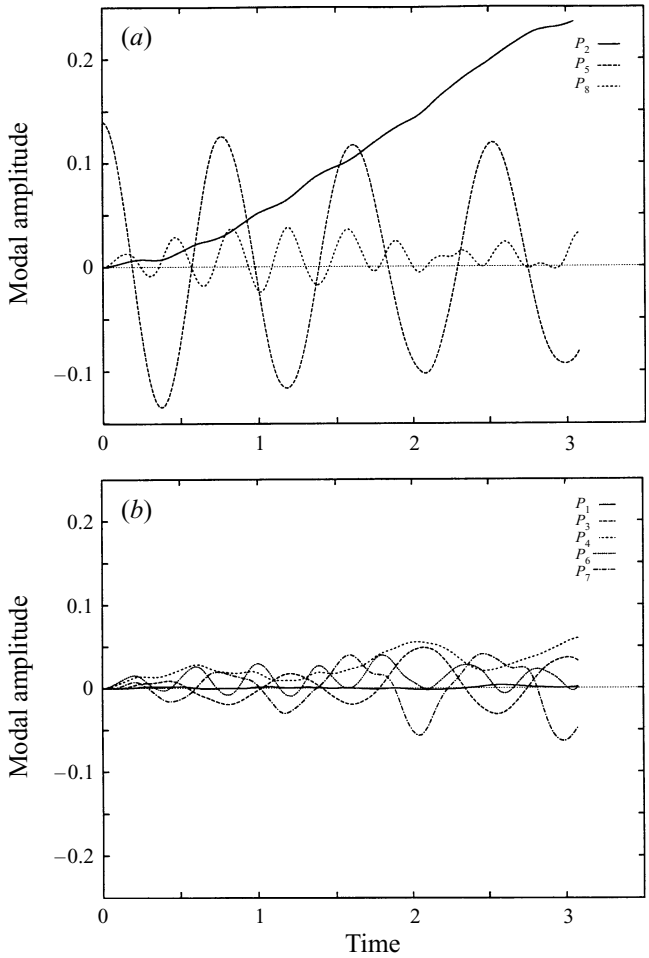

FIGURE 2. Modal amplitudes as functions of time for an initial fifth-mode perturbation of a charged drop with $Q_{FL} = 23$. (*a*) P_2, P_5, and P_8 modes, (*b*) P_1, P_3, P_4, P_6, and P_7 modes.

initial shape perturbation of the P_5 mode as small as 0.05 in amplitude will lead to the unbounded growth of the P_2 mode. The amplitudes from P_1 to P_7 modes are shown in figure 4 as functions of time. We note in particular that the initial perturbation in the fifth mode does not lead to the growth of the fifth mode; the amplitude of the fifth mode remains small. The drop develops instability through the growth of the second mode. Such a mechanism for instability is different from the well-known nonlinear instability mechanism, where subcritical transition to instability occurs when the the initial perturbation of the *linearly stable mode* has exceeded a threshold value. This latter scenario is shown in figure 5 which plots the amplitudes of the P_2 mode as functions of time when the initial perturbation amplitude of the P_2 mode has values 0.05, 0.10, 0.15, 0.18, and 0.20. We observe that unbounded growth of the second mode occurs when the initial perturbation of the second mode is about 0.18 or above. In contrast, the unbounded growth of the second mode shown in figure 4(*a*) is not caused by a finite-amplitude perturbation of the second mode but by a finite-amplitude perturbation of the fifth mode. While the second mode grows unbounded, the initial perturbation of the fifth mode does not.

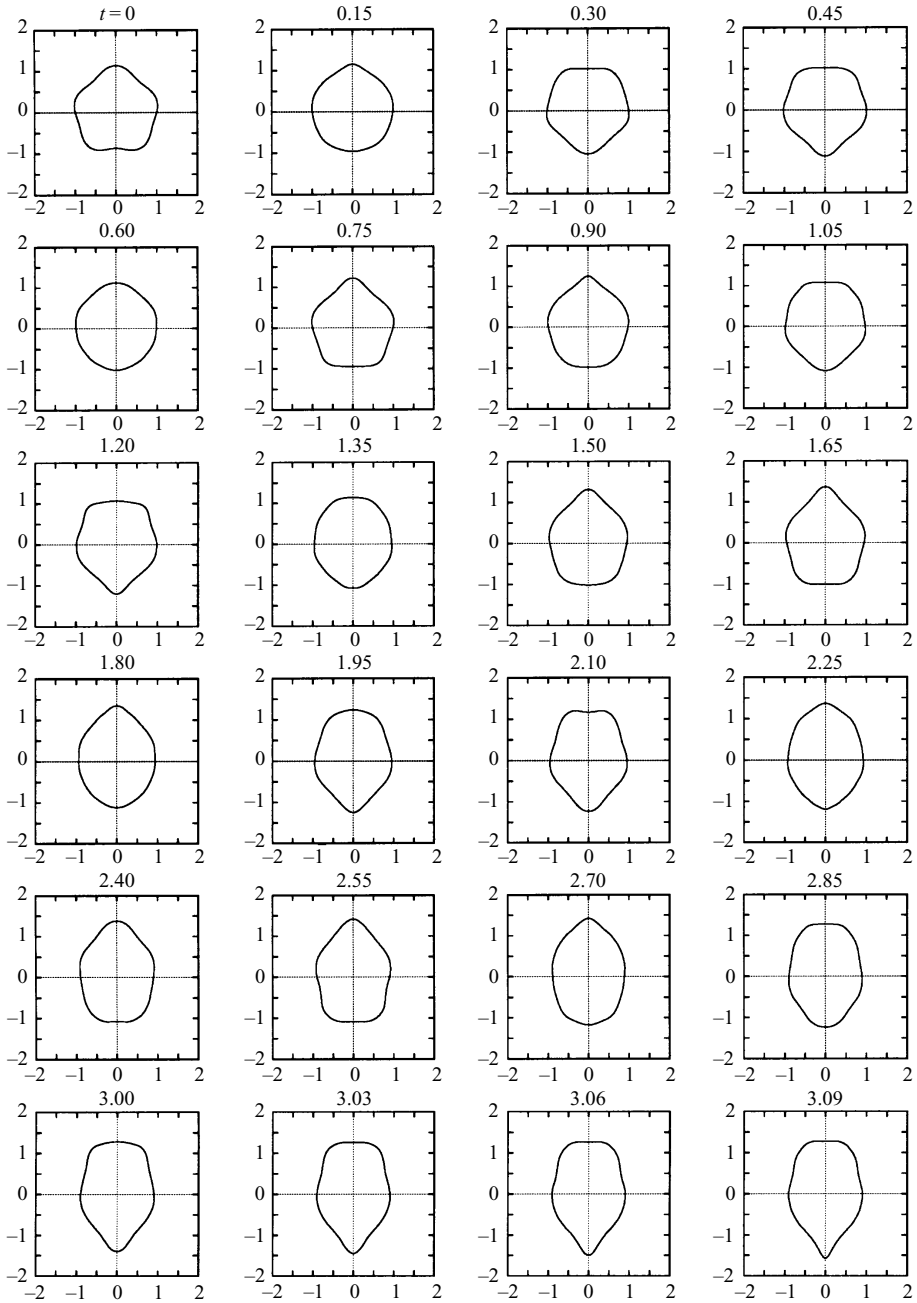

FIGURE 3. Shapes of a charged drop with $Q_{FL} = 23$ at equal time intervals after it is subjected to a perturbation in the fifth mode. The time intervals for the last three shapes are different.

Although we show here several simulation results for initial perturbations in the P_5 mode, simulations with initial perturbations in other modes have been done with similar results. Figure 6 shows the amplitudes of the P_2, P_4, P_6, and P_8 modes as functions of time. The initial shape perturbation is in the P_6 mode. Since the initial perturbation is an even mode, none of the odd modes are excited.

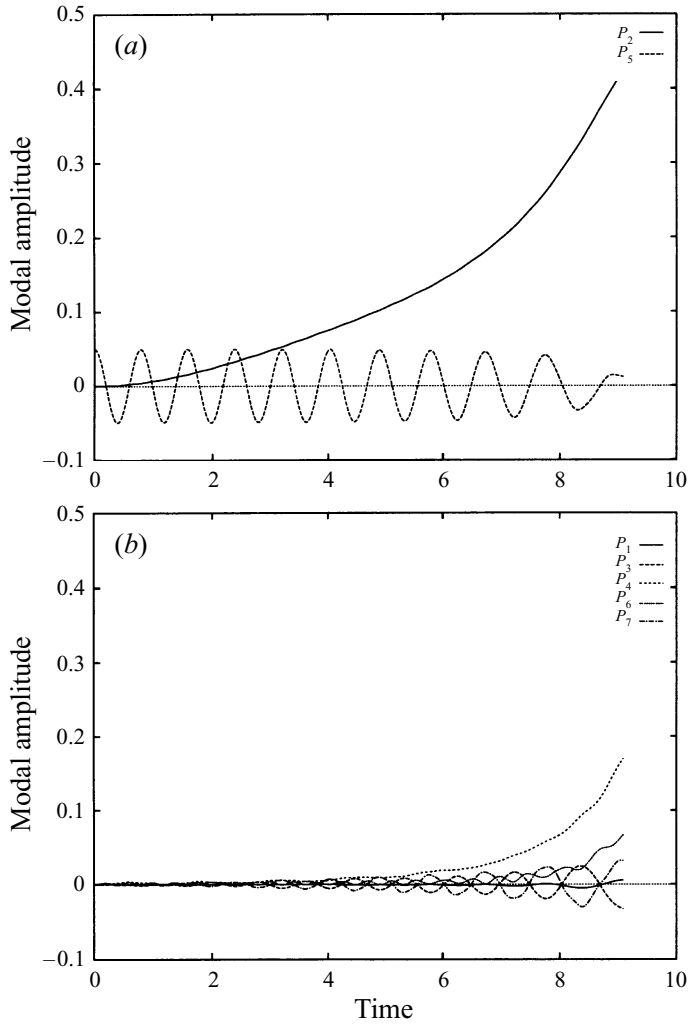

FIGURE 4. The amplitudes of the shape oscillation modes as functions of time for a charged drop with $Q_{FL} = 24.5$. The drop is subjected to an initial shape perturbation in the fifth mode with an amplitude of 0.05. (*a*) P_2 and P_5 modes, (*b*) P_1, P_3. P_4, P_6, and P_7 modes.

In summary, our numerical simulation indicates that the fundamental mode and the other shape modes couple with each other. This coupling is significant especially for drops which have electric charges near the Rayleigh limit. As a result of such modal coupling, a drop which is linearly stable can become unstable. To achieve some theoretical understanding of these observations, we use perturbation analysis to obtain amplitude equations to study this coupling phenomenon and the mechanism for instability.

4. Perturbation analysis

Following Tsamopoulos *et al.* (1985), we use the method of domain perturbations and multiple-scale analysis to derive the so-called amplitude equations for the

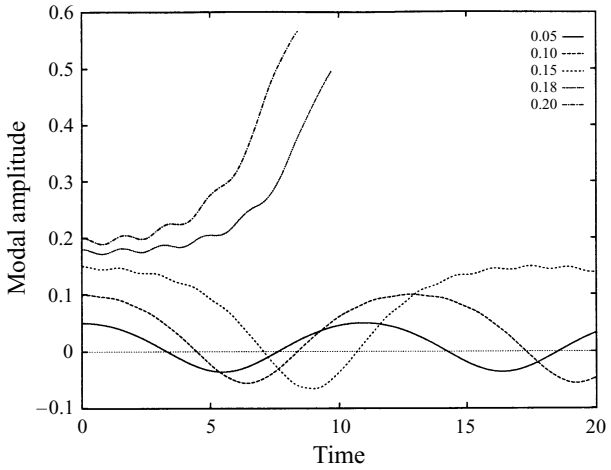

FIGURE 5. The amplitudes of the P_2 mode as functions of time when the drop is subjected to initial shape perturbations in the P_2 mode with respective amplitudes indicated in the figure. The electric charge of the drop is $Q_{FL} = 24.5$.

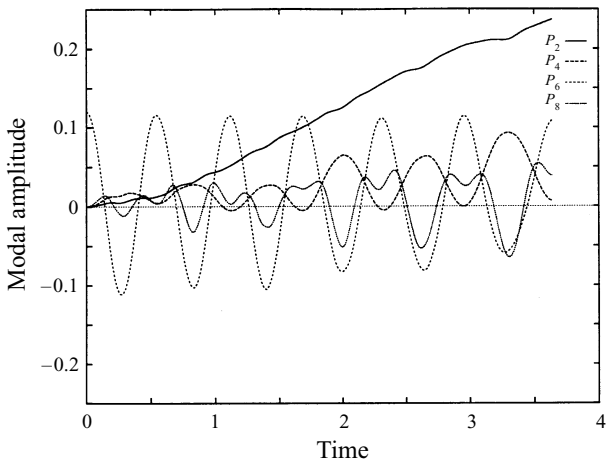

FIGURE 6. The amplitudes of the P_2, P_4, P_6, and P_8 modes when the drop is subjected to an initial shape perturbation in the P_6 mode. The electric charge of the drop is $Q_{FL} = 23$.

modes that are non-resonantly coupled. Tsamopoulos *et al.* employ the following expansions:

$$\phi = \epsilon\phi_1 + \epsilon^{3/2}\phi_{3/2} + \epsilon^2\phi_2, \tag{4.1}$$

$$F = 1 + \epsilon f_1 + \epsilon^{3/2} f_{3/2} + \epsilon^2 f_2, \tag{4.2}$$

$$V = V_0 + \epsilon V_1 + \epsilon^{3/2} V_{3/2} + \epsilon^2 V_2, \tag{4.3}$$

$$Q = Q_0 + \epsilon Q_1, \tag{4.4}$$

$$\Delta P_0 = \epsilon p_1 + \epsilon^{3/2} p_{3/2} + \epsilon^2 p_2, \tag{4.5}$$

where $Q_0 = Q_R^{(2)}$. Although we essentially follow the steps in Tsamopoulos *et al.* (1985), our treatment of the curvature term differs slightly. We use the following relationship:

$$2\nabla_s \cdot \boldsymbol{n} = 2 - (2f_1 + \nabla_s^2 f_1)\epsilon - [(2f_2 + \nabla_s^2 f_2) - 2f_1(f_1 + \nabla_s^2 f_1)]\epsilon^2 + \text{HOT}$$

where

$$\nabla_s^2 = \frac{\partial}{\partial \eta}\left[(1-\eta^2)\frac{\partial}{\partial \eta}\right],$$

$\eta = \cos\theta$ and HOT denotes higher-order terms. It can be shown that

$$\nabla_s^2(fg) = 2(1-\eta^2)\frac{\partial f}{\partial \eta}\frac{\partial g}{\partial \eta} + g\nabla_s^2 f + f\nabla_s^2 g.$$

In particular,

$$(\nabla_s^2 + 2)P_n = -(n-1)(n+2)P_n$$

where P_n is the nth-order Legendre polynomial.

When equations (4.1)–(4.5) are substituted into (2.1)–(2.8), the governing equations and the boundary conditions at different orders of ϵ are obtained. The solution at $O(1)$ is simply the equilibrium solution for an electrostatically charged sphere:

$$V_0 = \frac{Q_0}{r}. \tag{4.6}$$

At $O(\epsilon)$ the equations are

$$\nabla^2 \phi_1 = 0 \qquad \text{for } r < 1, \tag{4.7}$$

$$\nabla^2 V_1 = 0 \qquad \text{for } r > 1, \tag{4.8}$$

and the boundary conditions are

$$\frac{\partial f_1}{\partial t} - \frac{\partial \phi_1}{\partial r} = 0, \tag{4.9}$$

$$\frac{\partial \phi_1}{\partial t} - \frac{1}{4\pi}\frac{\partial V_0}{\partial r}\left[\frac{\partial V_1}{\partial r} + f_1\frac{\partial^2 V_0}{\partial r^2}\right] - (2 + \nabla_s^2)f_1 = p_1, \tag{4.10}$$

$$\int_0^\pi \left[\frac{\partial V_1}{\partial r} + f_1\left(\frac{\partial^2 V_0}{\partial r^2} + 2\frac{\partial V_0}{\partial r}\right)\right]\sin\theta\,\mathrm{d}\theta = -2Q_1, \tag{4.11}$$

$$\frac{\partial V_1}{\partial \theta} + \frac{\partial V_0}{\partial r}\frac{\partial f_1}{\partial \theta} = 0. \tag{4.12}$$

Since we are mainly interested in the coupling between the P_2 mode and another shape mode P_n, the solutions at $O(\epsilon)$ are assumed to be

$$f_1 = x_2(T_{1/2})P_2 + \tfrac{1}{2}\left[z_n(T)\mathrm{e}^{\mathrm{i}\omega_n t} + z_n(T)^*\mathrm{e}^{-\mathrm{i}\omega_n t}\right]P_n, \tag{4.13}$$

$$\phi_1 = \frac{\mathrm{i}}{2n}\omega_n\left[z_n(T)\mathrm{e}^{\mathrm{i}\omega_n t} - z_n(T)\mathrm{e}^{-\mathrm{i}\omega_n t}\right]r^n P_n, \tag{4.14}$$

$$V_1 = \frac{Q_1}{r} + Q_0 x_2(T_{1/2})r^{-3}P_2 + \frac{Q_0}{2}\left[z_n(T)\mathrm{e}^{\mathrm{i}\omega_n t} + z_n(T)^*\mathrm{e}^{-\mathrm{i}\omega_n t}\right]r^{-(n+1)}P_n, \tag{4.15}$$

where

$$\omega_n^2 = n(n-1)\left[n + 2 - \frac{Q_0^2}{4\pi}\right]. \tag{4.16}$$

Note that x_2 is assumed to be a function of the slow time $T_{1/2}$ and z_n is assumed to be a function of the slow time T, where

$$T_{1/2} = \epsilon^{1/2} t, \qquad T = \epsilon t.$$

At $O(\epsilon^{3/2})$, the equations are

$$\nabla^2 \phi_{3/2} = 0 \qquad \text{for } r < 1, \tag{4.17}$$

$$\nabla^2 V_{3/2} = 0 \qquad \text{for } r > 1, \tag{4.18}$$

and the boundary conditions are

$$\frac{\partial f_{3/2}}{\partial t} - \frac{\partial \phi_{3/2}}{\partial r} = -\frac{\partial f_1}{\partial T_{1/2}}, \tag{4.19}$$

$$\frac{\partial \phi_{3/2}}{\partial t} - \frac{1}{4\pi}\frac{\partial V_0}{\partial r}\left[\frac{\partial V_{3/2}}{\partial r} + f_{3/2}\frac{\partial^2 V_0}{\partial r^2}\right] - (2 + \nabla_s^2) f_{3/2} = p_{3/2}, \tag{4.20}$$

$$\int_0^\pi \left[\frac{\partial V_{3/2}}{\partial r} + f_{3/2}\left(\frac{\partial^2 V_0}{\partial r^2} + 2\frac{\partial V_0}{\partial r}\right)\right] \sin\theta \mathrm{d}\theta = 0, \tag{4.21}$$

$$\frac{\partial V_{3/2}}{\partial \theta} + \frac{\partial V_0}{\partial r}\frac{\partial f_{3/2}}{\partial \theta} = 0. \tag{4.22}$$

The solutions at $O(\epsilon^{3/2})$ are

$$f_{3/2} = 0, \tag{4.23}$$

$$\phi_{3/2} = \frac{1}{2}\frac{\partial x_2}{\partial T_{1/2}} r^2 P_2, \tag{4.24}$$

$$V_{3/2} = 0. \tag{4.25}$$

At $O(\epsilon^2)$ the equations are

$$\nabla^2 \phi_2 = 0 \qquad \text{for } r < 1, \tag{4.26}$$

$$\nabla^2 V_2 = 0 \qquad \text{for } r > 1, \tag{4.27}$$

and the boundary conditions are

$$\frac{\partial f_2}{\partial t} - \frac{\partial \phi_2}{\partial r} = f_1 \frac{\partial^2 \phi}{\partial r^2} - (1 - \eta^2)\frac{\partial f_1}{\partial \eta}\frac{\partial \phi_1}{\partial \eta} - \frac{\partial f_1}{\partial T} - \frac{\partial f_{3/2}}{\partial T_{1/2}}, \tag{4.28}$$

$$\begin{aligned}
&\frac{\partial \phi_2}{\partial t} - \frac{1}{4\pi}\frac{\partial V_0}{\partial r}\left(\frac{\partial V_2}{\partial r} + f_2 \frac{\partial^2 V_0}{\partial r^2}\right) - (2 + \nabla_s^2) f_2 \\
&\quad = -2 f_1 (f_1 + \nabla_s^2 f_1) - \frac{\partial^2 \phi_1}{\partial t \partial r} f_1 + \frac{1}{2}\left[\left(\frac{\partial \phi_1}{\partial r}\right)^2 + (1 - \eta^2)\left(\frac{\partial \phi_1}{\partial \eta}\right)^2\right] \\
&\qquad + \frac{1}{8\pi}\left(\frac{\partial V_1}{\partial r} + f_1 \frac{\partial^2 V_0}{\partial r^2}\right)^2 + \frac{1}{8\pi}\frac{\partial V_0}{\partial r}\left[-(1 - \eta^2)\left(\frac{\partial f_1}{\partial \eta}\right)^2 \frac{\partial V_0}{\partial r}\right. \\
&\qquad \left. + 2 f_1 \frac{\partial^2 V_1}{\partial r^2} + f_1^2 \frac{\partial^3 V_0}{\partial r^3} - 2(1 - \eta^2)\frac{\partial f_1}{\partial \eta}\frac{\partial V_1}{\partial \eta}\right] - \frac{\partial \phi_1}{\partial T} - \frac{\partial \phi_{3/2}}{\partial T_{1/2}},
\end{aligned} \tag{4.29}$$

$$\int_0^\pi \left[\frac{\partial V_2}{\partial r} + f_2\left(\frac{\partial^2 V_0}{\partial r^2} + 2\frac{\partial V_0}{\partial r}\right) + f_1^2\left(\frac{1}{2}\frac{\partial^3 V_0}{\partial r^3} + 2\frac{\partial^2 V_0}{\partial r^2} + \frac{\partial V_0}{\partial r}\right) + 2f_1\frac{\partial V_1}{\partial r}\right]\sin\theta \mathrm{d}\theta = 0, \tag{4.30}$$

$$\frac{\partial V_2}{\partial \theta} + \frac{\partial V_0}{\partial r}\frac{\partial f_2}{\partial \theta} + f_1\frac{\partial f_1}{\partial \theta}\left(-\frac{\partial V_0}{\partial r} + \frac{\partial^2 V_0}{\partial r^2}\right) + \frac{\partial f_1}{\partial \theta}\frac{\partial V_1}{\partial r} + f_1\frac{\partial^2 V_1}{\partial r \partial \theta} - f_1\frac{\partial V_1}{\partial \theta} = 0. \tag{4.31}$$

Following the procedures of multiple-scale analysis, we want to substitute f_1, ϕ_1, V_1, $f_{3/2}$, $\phi_{3/2}$, and $V_{3/2}$ into the right-hand sides of the above equations to isolate the secular terms. It is more convenient, however, to first simplify boundary conditions (4.28)–(4.31). First of all, we regard (4.30) as a constraint on the monopole term of V_2. That is, if we let

$$V_2 = \frac{q}{r} + \overline{V}_2$$

where $\overline{V}_2$ contains all terms excluding the monopole term, equation (4.30) is satisfied provided that

$$q = \frac{1}{2}\int_0^\pi \left[f_2\left(\frac{\partial^2 V_0}{\partial r^2} + 2\frac{\partial V_0}{\partial r}\right) + f_1^2\left(\frac{1}{2}\frac{\partial^3 V_0}{\partial r^3} + 2\frac{\partial^2 V_0}{\partial r^2} + \frac{\partial V_0}{\partial r}\right) + 2f_1\frac{\partial V_1}{\partial r}\right]\sin\theta\,\mathrm{d}\theta,$$

In other words, (4.30) does not enter the solvability conditions that we are seeking.

Next, we try to remove all non-homogeneous terms in equation (4.31) by letting

$$f_2 = \overline{f}_2 + \tilde{f}_2$$

where

$$\tilde{f}_2 = -\left(\frac{\partial V_0}{\partial r}\right)^{-1}\left[\frac{1}{2}\frac{\partial^2 V_0}{\partial r^2}f_1^2 + f_1\frac{\partial V_1}{\partial r}\right] \qquad (r = 1).$$

Thus the governing partial differential equations remain the same and the boundary conditions become

$$\frac{\partial \overline{f}_2}{\partial t} - \frac{\partial \phi_2}{\partial r} = -\frac{\partial \tilde{f}_2}{\partial t} + f_1\frac{\partial^2 \phi}{\partial r^2} - (1-\eta^2)\frac{\partial f_1}{\partial \eta}\frac{\partial \phi_1}{\partial \eta} - \frac{\partial f_1}{\partial T} - \frac{\partial f_{3/2}}{\partial T_{1/2}}, \tag{4.32}$$

$$\begin{aligned}\frac{\partial \phi_2}{\partial t} - \frac{1}{4\pi}\frac{\partial V_0}{\partial r}\left[\frac{\partial \overline{V}_2}{\partial r} + \overline{f}_2\frac{\partial^2 V_0}{\partial r^2}\right] - (2+\nabla_s^2)\overline{f}_2 \\ = \frac{1}{4\pi}\frac{\partial V_0}{\partial r}\frac{\partial^2 V_0}{\partial r^2}\tilde{f}_2 + (2+\nabla_s^2)\tilde{f}_2 - 2f_1(f_1 + \nabla_s^2 f_1) - \frac{\partial^2 \phi_1}{\partial t \partial r}f_1 \\ - \frac{1}{2}\left[\left(\frac{\partial \phi_1}{\partial r}\right)^2 + (1-\eta^2)\left(\frac{\partial \phi_1}{\partial \eta}\right)^2\right] + \frac{1}{8\pi}\left(\frac{\partial V_1}{\partial r} + f_1\frac{\partial^2 V_0}{\partial r^2}\right)^2 \\ + \frac{1}{8\pi}\frac{\partial V_0}{\partial r}\left[-(1-\eta^2)\left(\frac{\partial f_1}{\partial \eta}\right)^2\frac{\partial V_0}{\partial r} + 2f_1\frac{\partial^2 V_1}{\partial r^2} + f_1^2\frac{\partial^3 V_0}{\partial r^3}\right. \\ \left. - 2(1-\eta^2)\frac{\partial f_1}{\partial \eta}\frac{\partial V_1}{\partial \eta}\right] - \frac{\partial \phi_1}{\partial T} - \frac{\partial \phi_{3/2}}{\partial T_{1/2}},\end{aligned} \tag{4.33}$$

$$\frac{\partial \overline{V}_2}{\partial \theta} + \frac{\partial V_0}{\partial r}\frac{\partial \overline{f}_2}{\partial \theta} = 0. \tag{4.34}$$

We substitute (4.13)–(4.15), (4.23)–(4.25) into the above boundary conditions. The right-hand side of (4.32) can be written as

$$A_2P_2 + (A_n e^{i\omega_n t} + A_n^* e^{-i\omega_n t})P_n + \text{nonsecular terms}.$$

The right-hand side of (4.33) can be written as

$$B_2P_2 + (B_n e^{i\omega_n t} + B_n^* e^{-i\omega_n t})P_n + \text{nonsecular terms}$$

where

$$A_2 = 0$$

$$A_n = \frac{i\omega_n}{2}\left\{\frac{Q_1}{Q_0}z_n + \left[(2n+1)N_1 - \frac{N_4}{n}\right]x_2 z_n + \frac{i}{\omega_n}\frac{dz_n}{dT}\right\},$$

$$B_2 = \left(\frac{4}{Q_0} + \frac{Q_0}{4\pi}\right)Q_1 x_2 + \frac{12}{7}x_2^2 + \left[\left(2 - 4n + n^2 + n^3 + \frac{\omega_n^2}{4}\right)N_2 + \left(1 - n - \frac{\omega_n^2}{4n^2}\right)N_3\right]|z_n|^2 - \frac{1}{2}\frac{d^2x_2}{dT_{1/2}^2},$$

$$B_n = \left[-1 + \frac{n}{2} + \frac{n^2}{2} - \frac{(1-n)Q_0^2}{8\pi}\right]\frac{Q_1}{Q_0}z_n + \left[\left(-2 + 4n + \frac{n^2}{2} + \frac{n^3}{2} + \frac{\omega_n^2}{2}\right)N_1 - nN_4\right]x_2 z_n - \frac{i\omega_n}{2n}\frac{dz_n}{dT}.$$

By requiring the solutions of $\overline{f}_2$, ϕ_2, and $\overline{V}_2$ to be bounded and following the derivations in Feng & Leal (1994), we obtain the solvability conditions

$$B_2 = 0,$$

$$\omega_n A_n - inB_n = 0,$$

from which we obtain

$$\frac{d^2x_2}{dT_{1/2}^2} = -\kappa x_2 + \tfrac{24}{7}x_2^2 + C|z_n|^2, \tag{4.35}$$

$$\frac{dz_n}{dT} = -i\sigma_n z_n - iDx_2 z_n, \tag{4.36}$$

where

$$\kappa = -16\frac{Q_1}{Q_0}, \tag{4.37}$$

$$\sigma_n = \frac{4n(n-1)Q_1}{\omega_n Q_0}, \tag{4.38}$$

$$C = \frac{15(n-1)(n+1)(n^2+3n-2)}{2(2n-1)(2n+1)(2n+3)}, \tag{4.39}$$

$$D = \frac{3n(n-1)(n+1)(n^2+3n-2)}{2(2n-1)(2n+3)\omega_n}. \tag{4.40}$$

Equations (4.35) and (4.36) describe the evolution of the modal amplitude of the second mode and the oscillatory modal amplitude of the nth mode. They are the amplitude equations that our subsequent analysis will be based on. When z_n is zero, (4.35) is identical to the one obtained by Tsamopoulos *et al.* (1985). Our definitions of κ and the coefficient of x_2^2 are also identical to theirs. Physically, κ is proportional to the excess electric charge above the Rayleigh limit with $\kappa > 0$ being subcritical. The nonlinear term $C|z_n|^2$ is due to the coupling by the nth mode. In (4.36), the nonlinear term $Dx_2 z_n$ is due to the coupling by the second mode. If x_2 is zero, (4.36) is linear. The physical meaning of σ_n becomes obvious if we substitute the solution of this equation $z_n(T) = z_n(0)e^{-\mathrm{i}\sigma_n T}$ into (4.13) to obtain

$$f_1 = \tfrac{1}{2} z_n(0) \left[\mathrm{e}^{\mathrm{i}(\omega_n - \epsilon\sigma_n)t} + \mathrm{e}^{-\mathrm{i}(\omega_n - \epsilon\sigma_n)t} \right] P_n. \tag{4.41}$$

Since the ω_n above is evaluated at the Rayleigh limit (cf. (4.16)), σ_n gives the frequency detuning due to the difference of the electric charge from the Rayleigh limit. Alternatively, it can be obtained by expanding the frequency as a function of the electric charge as follows:

$$\omega_n(Q_0 + \epsilon Q_1) = \omega_n(Q_0) - \epsilon\sigma_n Q_1 + O(\epsilon^2).$$

The σ_n obtained by the above expansion agrees with that in formula (4.38).

5. Analysis of the amplitude equations

We now attempt to achieve a qualitative understanding of (4.35) and (4.36). Equation (4.35) has been analysed by Tsamopoulos *et al.* (1985) for the case $z_n = 0$, and we shall discuss our results in the context of theirs in the following two paragraphs.

A transcritical bifurcation is shown to occur at $\kappa = 0$, i.e. at $Q = Q_R^{(2)}$. For the electric charge below the Rayleigh limit, the phase-plane diagram for x_2 is shown schematically in figure 7. (A more accurate figure is given in figure 2 of Tsamopoulos *et al.* 1985.) There exist two equilibria: one is a saddle and the other a centre. A homoclinic orbit H encloses a region in which the motion is periodic. Outside the region, the motion is unbounded which implies the breakup of the drop. Our numerical simulation results in figure 5 contain both types of motion. For initial conditions $x_2 = 0.18$, and $x_2 = 0.20$, the motions are unbounded. For smaller initial perturbations, the motions are periodic. Note that since our simulation is done on the full partial differential equations, we also see small wiggles on curves corresponding to relatively large initial perturbations (0.15, 0.18, 0.20); these wiggles represent the higher modes which are excited by the low modes when the amplitudes of the latter are sufficiently large.

If we plot the two equilibria as we vary the surface electric charge, we obtain two straight lines (one coincides with the horizontal axis) on the bifurcation diagram shown in figure 8. In this figure, the horizontal axis is $-\kappa$, which is proportional to the electric charge in excess of the Rayleigh limit; the left-hand side is subcritical. The vertical axis is the value of x_2 at the equilibrium. On the left half of the figure, $\kappa > 0$, the electric charge is below the Rayleigh limit. The spherical shape of the drop $x_2 = 0$ is stable and the prolate shape $x_2 = \frac{7}{24}\kappa$ is unstable. On the right half of the figure, $\kappa < 0$, the electric charge is above the Rayleigh limit. The spherical shape $x_2 = 0$ is unstable and the oblate shape $x_2 = -\frac{7}{24}|\kappa|$ is stable. However, it is shown by Natarajan & Brown (1987) that the oblate spheroidal shape is unstable to non-axisymmetric perturbations.

Now let us examine the case when $z_n \neq 0$. We first make the observation that

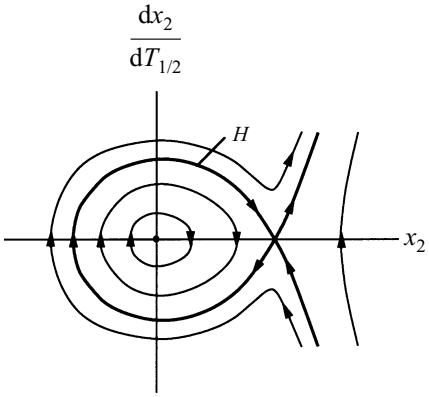

FIGURE 7. Orbits in the phase-plane (x_2, $dx_2/dT_{1/2}$) for a subcritically charged drop. The origin corresponds to a stable spherical shape. The saddle corresponds to the unstable prolate equilibrium shape of the drop.

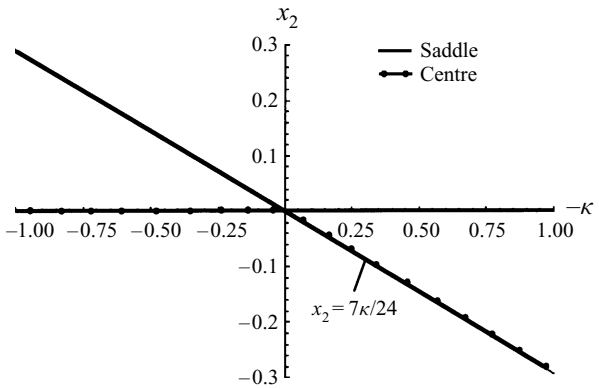

FIGURE 8. The bifurcation diagram of the equilibrium solutions of a charged drop near the Rayleigh limit.

according to (4.36), the amplitude $|z_n|$ is a constant. This becomes obvious if we let $z_n = r_n e^{i\theta_n}$; (4.36) then take the form

$$\dot{r}_n = 0, \tag{5.1}$$

$$\dot{\theta}_n = -(\sigma_n + Dx_2). \tag{5.2}$$

Therefore, we treat $|z_n|$ as a constant in the following analysis. This treatment of $|z_n|$ is also consistent with the numerical simulation results. For instance, in figure 4(*a*), we see that the P_5 mode oscillation amplitude hardly changes before x_2 experiences large increases. Note that it is the P_5 mode *oscillation amplitude* that is related to the slow time variable z_n.

Treating $|z_n|$ as a constant, we study the equilibrium solutions of (4.35) and the stability of these solutions. The equilibrium solutions of (4.35) are given by the solutions of the quadratic equation

$$-\kappa x_2 + \tfrac{27}{4}x_2^2 + C|z_n|^2 = 0.$$

Depending on the values of κ and $C|z_n|^2$, we can have two, one or zero solutions. In

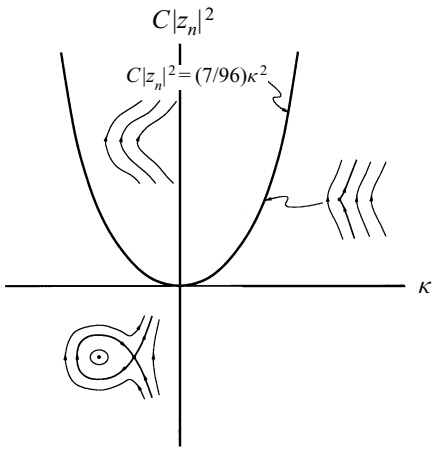

FIGURE 9. The bifurcation set and the corresponding phase portraits of equation (4.35).

the parameter space (κ, $C|z_n|^2$), a parabola $C|z_n|^2 = \frac{7}{96}\kappa^2$ separates the space into two regions. Inside the parabola, there is no equilibrium solution. Outside the parabola, there are two equilibrium solutions given by

$$x_2 = \tfrac{1}{2}\left(\kappa \pm [\kappa^2 - \tfrac{96}{7}C|z_n|^2]^{1/2}\right).$$

On the parabola, there is only one solution. This partition of the parameter space, also called the bifurcation set, is given in figure 9.

If we multiply (4.35) by $\mathrm{d}x_2/\mathrm{d}T_{1/2}$ and integrate with respect to $T_{1/2}$, we obtain the following constant of motion:

$$\left(\frac{\mathrm{d}x_2}{\mathrm{d}T_{1/2}}\right)^2 + \tfrac{1}{2}\kappa x_2^2 - \tfrac{8}{7}x_2^3 - C|z_n|^2 x_2 = \text{const.}$$

By plotting the level curves of the above constant of motion, we obtain the phase portraits in the phase space (x_2, $\mathrm{d}x_2/\mathrm{d}T_{1/2}$). The phase portraits are the same within each region identified above. These are shown schematically in figure 9.

From figure 9, we observe that there is only one phase portrait corresponding to negative C. Under such circumstances, there are always two equilibrium solutions, one a saddle and the other a centre. The presence of z_n does not have a qualitative effect on the dynamics of x_2. We plot the equilibrium solutions as functions of $-\kappa$ in figure 10(a). There is no bifurcation associated with the two branches of the equilibrium solutions.

According to (4.39), C is positive. Therefore for the dynamics of a charged liquid drop, the presence of z_n can change the dynamics of x_2 qualitatively. Specifically, for a fixed value of z_n, figure 9 shows that there is an open interval of κ ($|\kappa| < \left(\frac{96}{7}C\right)^{1/2}|z_n|$) on which no equilibrium solution exists. The bifurcation diagram corresponding to this case is shown in figure 10(b). We see that the two equilibrium solutions, a saddle and a centre, disappear through saddle-node bifurcations.

We conclude from the study above that the presence of a high-mode shape perturbation changes the bifurcation type at the Rayleigh limit from a transcritical to a saddle-node bifurcation. Thus this creates an open interval for Q on which no stable equilibrium exists. Consequently, an initial shape perturbation of a high mode can lead to the instability of the drop shape oscillation of the fundamental mode. This fact is important since according to the linear stability theory, the drop is stable

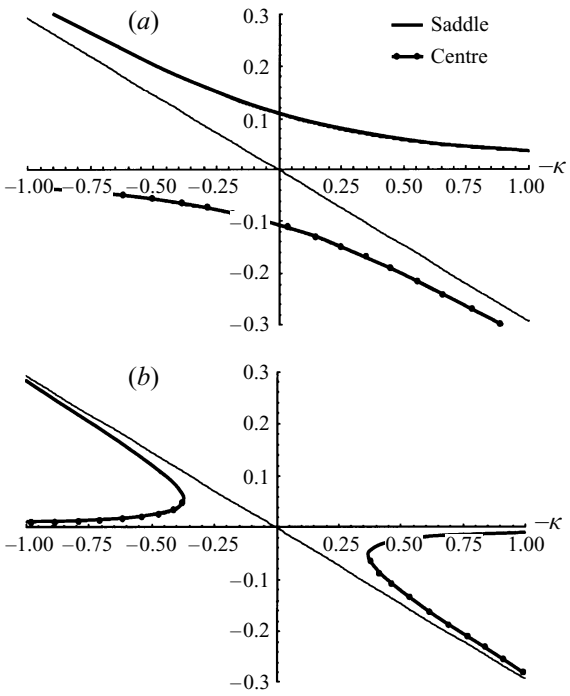

FIGURE 10. The bifurcation diagrams of equilibrium solutions for two different cases. (*a*) $C < 0$, (*b*) $C > 0$.

under-small-amplitude shape perturbation. This instability is totally a consequence of the nonlinear modal interaction effect.

6. Discussion

For the electric charge below the Rayleigh limit, the spherical equilibrium shape of the drop is stable according to the linear stability theory. However, the spherical shape can become unstable under finite perturbations. Figures 5 and 7 show that if the perturbation amplitude of the second mode is above a certain threshold value, the stability is lost. This type of nonlinear instability is well-known (Basaran *et al.* 1995; Drazin & Reid 1981).

Here, however, we have identified another mechanism for nonlinear instability. That is, instability sets in through nonlinear coupling between non-resonant modes. The difference from the above one is that the initial perturbation is not on the second mode but on another shape mode, the fifth mode for instance. Without the nonlinear coupling to the second mode, according to the well-known nonlinear instability mechanism the fifth mode could become unstable if the perturbation were large enough. But such is not the case. The initial perturbation of the fifth mode is not large enough to cause the fifth mode to be unstable. Yet its nonlinear coupling to the second mode causes the second mode to be unstable. This is evident in our numerical simulation results; in figures 2(*a*) and 4(*a*) the amplitude of the fifth mode does not grow at all while the second mode grows rapidly.

In reality, whether a high-mode shape perturbation will lead to the unbounded growth of the fundamental mode is also dependent on the viscosity of the fluid. In both the numerical simulation and the perturbation analysis, we have not included fluid vis-

cosity. This limits the applicability of our results. Needless to say, for drops with large diameters such as the ones that can be achieved in zero gravity, our result is applicable. Even for drops whose viscosity is not negligible, periodic forcing can be applied to sustain constant-amplitude shape oscillation of the high mode. In that case, the shape oscillation can become unstable due to the coupling to the fundamental mode.

Despite the limitation of the inviscid assumption in our analysis, a very important mechanism for nonlinear instability has been identified. It is safe to say that this new mechanism plays an important role in many other instability phenomena involving fluid flows. In order to see such a connection, we first note that (4.35) can be written in the following equivalent form:

$$\dot{\boldsymbol{x}} = \begin{bmatrix} 0 & 1 \\ -\kappa & 0 \end{bmatrix} \boldsymbol{x} + \text{nonlinear terms},$$

where $\boldsymbol{x} = \{x_2,\ \mathrm{d}x_2/\mathrm{d}T_{1/2}\}^T$ and the dot stands for derivative with respect to $T_{1/2}$. If κ is a small positive number, the linear coefficient matrix has a pair of pure imaginary eigenvalues. However, as κ becomes increasingly small, the coefficient matrix approaches a type of matrix defined as non-normal (Kato 1976). The non-normal degeneracy has been shown to occur in the operators that arise in Poiseuille and Couette flow in Reddy, Schmidt & Henningson (1993). By calculating the pseudospectra of the non-normal operators, Trefethen *et al.* (1993) propose an explanation for the anomalies of subcritical transition to turbulence in Poiseuille and Couette flow. The present work suggests that the presence of high modes may serve as perturbations which destablize the shear flows.

As another example, we recall that the linear operator governing the dynamics of a gas or a vapour bubble has similar degeneracy. Physically, this degeneracy arises because the translational motion of the bubble centroid has zero frequency. It is shown in Feng & Leal (1995) that the coupling of this mode to two shape oscillation modes leads to the erratic dancing of the bubble (Benjamin & Ellis 1990).

In the context of nonlinear wave-wave interactions, the new type of non-resonant modal coupling implies that short waves may interact with long waves. It has been observed (Mahony & Smith 1972) that standing surface waves in water may be excited by acoustic fields of very much higher frequency. Some aspects of such wave–wave interactions have been investigated numerically by Olmez & Milgram (1995). Our discussion in this work has been limited to the effect on the fundamental mode of the fast mode. Examining (4.36), we note that the slow mode also affects the fast mode through the nonlinear term $-\mathrm{i}Dx_2z_n$. If x_2 were constant, this term would change the frequency of the nth mode. In the case of charged drops, D is positive according to (4.40), and for positive x_2 the fast mode slows down. This is manifested in figure 4(a) by the slowing down of the fifth mode when the amplitude of the second mode becomes large. Although this frequency change is very small, its effect can be significant when the fast mode is *resonantly* interacting with a third mode as is the case studied by Olmez & Milgram.

Our analysis also reveals that the coupling coefficient C in (4.35) determines whether the high-mode perturbation will lead to the instability of the low mode. For $C < 0$, figure 10(a), the high mode does not affect the dynamics of the low mode in a qualitative way. On the other hand, for $C > 0$ as is the case for the charged drops, the high mode does change the dynamics of the low mode in a dramatic fashion. Therefore the coupling coefficient C is a very important quantity in nonlinear stability analysis.

Finally, we comment that in a sense the coupling analysed in this paper can also be called resonant since at the Rayleigh limit the frequency of the second mode is zero, which can be considered in resonance with any mode. We use the term non-resonant to distinguish from commonly studied one-to-one, one-to-two, and one-to-three resonances. This type of nonlinear modal coupling was first studied by Nayfeh & Nayfeh (1992) in structural systems. For structural systems, which typically have cubic nonlinearity, the mechanism for the coupling is found to be caused by the *cross-softening* effect of the fast mode on the slow mode (Feng 1995). In other words, the motion of the fast mode leads to a decrease in the oscillation frequency and eventual instability of the slow mode. The present work shows that the coupling in fluid systems which typically have quadratic nonlinearity differs from that.

In conclusion, we find that the shape oscillation modes of a charged conducting drop can couple to each other although their natural frequencies are nowhere close to the often-studied one-to-one, one-to-two, or one-to-three resonances. This coupling gives rise to a new mechanism for nonlinear instability: the perturbation of a high mode causes a low mode to become unstable while the high mode remains stable.

The author would like to express his gratitude to the referees for their valuable suggestions and to Professor C. C. Mei for bringing the paper of Mahony & Smith to his attention. This work is supported by the MIT Sea Grant College Program in the form of a Doherty Professorship.

REFERENCES

Basaran, O. A., Patzek, T. W., Benner, R. E. & Scriven, L. E. 1995 Nonlinear oscillations and breakup of conducting, inviscid drops in an externally applied electric field. *Ind. Engng Chem. Res.* **34**, 3454–3465.

Basaran, O. A. & Scriven, L. E. 1989 Axisymmetric shapes and stability of isolated charged drops. *Phys. Fluids* A **1**, 795–798.

Benjamin, T. B. & Ellis, A. T. 1990 Self-propulsion of asymmetrically vibrating bubbles. *J. Fluid Mech.* **212**, 65–80.

Brebbia, C. A., Telles, J. C. F. & Wrobel, L. C. 1984 *Boundary Element Techniques: Theory and Applications in Engineering*. Springer.

Drazin, P. G. & Reid, W. H. 1981 *Hydrodynamic Stability*. Cambridge University Press.

Feng, Z. C. 1995 Nonresonant modal interactions. *Symp. on Nonlinear Vibrations at the 15th ASME Biennial Conference on Mechanical Vibration and Noise, September 17–21, 1995, Boston, MA.* pp. 511–517.

Feng, Z. C. & Leal, L. G. 1993 Energy transfer mechanism in coupled bubble oscillations. *Phys. Fluids* A **5**, 826–836.

Feng, Z. C. & Leal, L. G. 1994 Bifurcation and chaos in shape and volume oscillations of a periodically driven bubble with two-to-one internal resonance. *J. Fluid Mech.* **266**, 209–242.

Feng, Z. C. & Leal, L. G. 1995 Translational instability of a bubble undergoing shape oscillations. *Phys. Fluids* A **7**, 1825–1336.

Feng, Z. C. & Leal, L. G. 1996 Numerical simulation of the dynamics of electrostatically levitated drop. *Intl J. Multiphase Flow* **22**, 93–120.

Ffowcs Williams, J. E. & Guo, Y. P. 1991 On resonant nonlinear bubble oscillations. *J. Fluid Mech.* **224**, 507–529.

Kato, K. 1976 *Perturbation Theory for Linear Operators*. Springer.

Mahony, J. J. & Smith, R. 1972 On a model representation for certain spatial-resonance phenomena. *J. Fluid Mech.* **53**, 193–207.

Mei, C. C. & Zhou, X. 1991 Parametric resonance of a spherical bubble. *J. Fluid Mech.* **229**, 29–50.

Natarajan, R. & Brown, R. A. 1986 Quadratic resonance in the three-dimensional oscillations of inviscid drops with surface tension. *Phys. Fluids* **29**, 2788–2797.

Natarajan, R. & Brown, R. A. 1987 The role of three-dimensional shapes in the break-up of charged drops. *Proc. R. Soc. Lond.* A **410**, 209–227.

Nayfeh, S. A. & Nayfeh, A. H. 1992 Energy transfer from high- to low-frequency modes in flexible structures. *Nonlinear Vibration.* ASME DE, Vol. 50/ AMD, Vol. 144, pp. 89–98.

Olmez, H. S. & Milgram, J. H. 1995 Nonlinear energy transfer to short gravity waves in the presence of long waves. *J. Fluid Mech.* **289**, 199–226.

Pelekasis, N. A., Tsamopoulos, J. A. & Manolis, G. D. 1990 Equilibrium shapes and stability of charged and conducting drops. *Phys. Fluids* A **2**, 1328–1340.

Rayleigh, Lord 1882 On the equilibrium of liquid conducting masses charged with electricity. *Phil. Mag.* **14**, 184–186.

Reddy, S. C., Schmid, P. H. & Henningson, D. S. 1993 Pseudospectra of the Orr-Sommerfeld operator. *SIAM J. Appl. Maths* **53**, 15–47.

Tsamopoulos, J. A., Akylas, T. R. & Brown, R. A. 1985 Dynamics of charged drop break-up. *Proc. R. Soc. Lond.* A **401**, 67–88.

Tsamopoulos, J. A. & Brown, R. A. 1984 Resonant oscillations of inviscid charged drops. *J. Fluid Mech.* **147**, 373–395.

Trefethen, L. N., Trefethen, A. E., Reddy, S. C. & Driscoll, T. A. 1993 Hydrodynamic stability without eigenvalues. *Science* **261**, 578–583.